Available online at www.sciencedirect.com

ScienceDirect

Ceramics International 40 (2014) 3855–3864

CERAMICS INTERNATIONAL

www.elsevier.com/locate/ceramint

Potentiostatically deposited polypyrrole/graphene decorated nano-manganese oxide ternary film for supercapacitors

Lim Y.S.[a], Tan Y.P.[a,b], Lim H.N.[a,c,*], Huang N.M.[d], Tan W.T.[a], Yarmo M.A.[e], Chun-Yang Yin[f]

[a]Department of Chemistry, Faculty of Science, Universiti Putra Malaysia, 43400 UPM, Serdang, Selangor, Malaysia
[b]Centre of Excellence for Catalysis Science and Technology, Faculty of Science, Universiti Putra Malaysia, 43400 UPM Serdang, Selangor, Malaysia
[c]Functional Device Laboratory, Institute of Advanced Technology, Universiti Putra Malaysia, 43400 UPM Serdang, Selangor, Malaysia
[d]Low Dimensional Materials Research Centre, Department of Physics, Faculty of Science, University of Malaya, 50603 Kuala Lumpur, Malaysia
[e]School of Chemical Sciences and Food Technology, Faculty of Science and Technology, Universiti Kebangsaan Malaysia, 43650 Bandar Baru Bangi, Selangor, Malaysia
[f]Chemical and Analytical Sciences, Murdoch University, Murdoch, 6150 WA, Australia

Received 18 May 2013; received in revised form 5 August 2013; accepted 5 August 2013
Available online 14 August 2013

Abstract

A simple method based on potentiostatic polymerization was developed for the preparation of ternary manganese oxide-based nanocomposite films. The ternary nanocomposites, which were characterized using x-ray diffraction spectroscopy and x-ray photoelectron spectroscopy, showed that the manganese oxide within the film consisted of MnO_2 and Mn_2O_3. Electrochemical measurements showed that the ternary nanocomposite electrode exhibited high specific capacitance (up to 320.6 F/g), which was attributed to the morphology of a polypyrrole/graphene/manganese-oxide (PPy/GR/MnO_x) ternary nanocomposite. The experimental approach maximized the pseudocapacitive contribution from redox-active manganese oxide (MnO_x) and polypyrrole (PPy), as well as the electrochemical double layer capacitive (EDLC) characteristic from graphene (GR) sheets. Long cyclic measurements indicated that the specific capacitance of the ternary nanocomposite film could retain 93% of its initial value over 1000 charge/discharge cycles, in the potential range of −0.2 to 0.7 V versus silver/silver chloride electrode (Ag/AgCl).

Keywords: Supercapacitor; Manganese oxide; Graphene; Polypyrrole

1. Introduction

Supercapacitors have received considerable attention owing to their expanding array of applications, especially in providing power to hybrid vehicles and portable electronics. As energy storage devices, supercapacitors bridge the gap between a conventional capacitor and a battery [1], and have been studied extensively. In this context, relentless efforts have been underway, especially in searching for novel electrode materials. Generally, there are three categories of electrode materials, i.e. carbon materials, metal oxides/hydroxides and conducting polymers. Depending on the electrode materials used, two types of supercapacitors can be constructed; namely, electric double layer capacitors (EDLC) and pseudocapacitors. Energy storage in an EDLC results from the separation of electronic and ionic charges between the electrode and electrolyte interface, while a pseudocapacitor utilizes Faradaic reactions occurring within the active material of electrodes [2,3].

Carbon materials such as activated carbon and carbon nanotubes (CNT) have been investigated widely for EDLC, owing to their good conductivity and excellent chemical properties [4]. Recently, the focus has been diverted to graphene-based materials since they have shown immense theoretical and practical advantages, such as a large surface area, excellent conductivity and capacitance, as well as relatively low production costs [5–8]. On the other hand, polypyrrole (PPy), which is an ideal candidate for pseudocapacitor electrode, is receiving considerable attention as a result of its high electrical properties [9], ease of preparation,

*Corresponding author at: Department of Chemistry, Faculty of Science, Universiti Putra Malaysia, 43400 UPM, Serdang, Selangor, Malaysia.
Tel.: +60 16 33 016 09.
E-mail address: hongngee@upm.edu.my (H.N. Lim).

0272-8842/$ - see front matter © 2013 Elsevier Ltd and Techna Group S.r.l. All rights reserved.
http://dx.doi.org/10.1016/j.ceramint.2013.08.026

good environment stability [10] and large specific capacitance [11]. Redox metal oxides such as RuO_2 and MnO_2 are also promising materials for pseudo-capacitors. Hydrous RuO_2 has been studied extensively, and its capacitance value was as high as 720 F/g in acidic electrolyte, although the drawback of this material is its high production cost and toxic nature [12]. To circumvent these disadvantages, researchers have focused on other cost-effective and 'green' electrode materials. Correspondingly, the electrochemical behavior of MnO_2 is also a subject of intensive investigation, owing to its good electrochemical performance [13,14]. Moreover, MnO_2 has attracted considerable attention thanks to its abundance and relatively environmentally friendly nature.

Numerous material types have been identified as promising materials for supercapacitor electrodes. In essence, each class has its distinctive advantages and disadvantages, in terms of supercapacitor application. For example, the electrostatic charge storage mechanism of the EDLC electrode has very high stability during charge–discharge cycling. However, electrodes of this kind only store limited charges, leading to low specific capacitance [15]. While transition metal oxides and conducting polymers have relatively high capacitance, the challenges remain because the relatively low mechanical stability and cycle life inhibit their application for supercapacitors [16]. Hence, the real current challenge in the synthesis of binary or ternary composites of carbon materials, conducting polymers and metal oxides as materials for supercapacitors, is therefore to leverage their unique advantages while, at the same time, minimizing their disadvantages.

Recently, efforts have been made to integrate nano-scale manganese oxide onto graphene; however, the nanocomposite exhibits specific capacitances within the 100–200 F/g [13–18]. Based on the findings, it has shown some improvement in maximizing the utilization of manganese oxide, but substantial improvements still have to be made for its successful commercialization.

In this study, a simple, fast and one-step electrochemical polymerization of polypyrrole/graphene/manganese oxide ($PPy/GR/MnO_x$) ternary nanocomposite films was conducted, whereby they are deposited potentiostatically in the presence of sodium *p*-toluenesulfonate (NapTS) as a supporting electrolyte. In our previous study, graphene oxide (GO) was electrodeposited with a pyrrole monomer from an aqueous solution to form a polypyrrole/graphene (PPy/GR) nanocomposite film. It has been shown that GO was reduced to graphene (GR) during the deposition process [19]. For the present study, $PPy/GR/MnO_x$ ternary nanocomposites were synthesized potentiostatically, with the addition of $MnSO_4$ in the deposition solution. The manganese oxide (MnO_x) particles were grown directly along the PPy and conducting graphene, which acted as spacers to maintain the detachment of neighboring sheets. The graphene sheets, coated with MnO_x particles and PPy, overlapped with each other, forming a three-dimensional (3D) conducting network that improved the contact between the electrode material and the electrolyte (Fig. 1). To the best of the authors' knowledge, the deposition of 3D structured MnO_x directly onto graphene and PPy has not been previously reported. The obtained nanocomposite exhibited a high specific capacitance and an excellent long cycle life.

2. Experimental

2.1. Materials

Graphite powder was obtained from Ashbury Graphite Mills Inc., code no. 3061. Sulfuric acid (H_2SO_4, 95–98%), phosphoric acid (H_3PO_4, 85%), potassium permanganate ($KMnO_4$, 99.9%) and hydrogen peroxide (H_2O_2, 30%) were purchased from Systerm, Malaysia. Hydrogen chloride (HCl, 37%) and manganese sulfate ($MnSO_4$, 98–101%) were purchased from Sigma-Aldrich and Merck, respectively. Pyrrole (99%, Acros Organic) was stored in 0 °C and distilled prior to use.

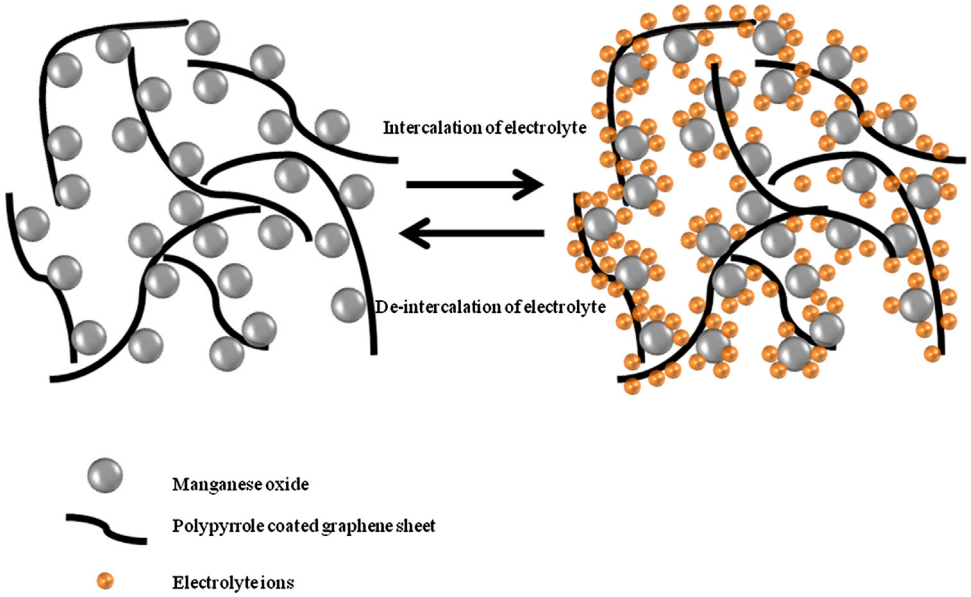

Fig. 1. 3D model of microstructure of ternary nanocomposite facilitating the diffusion of electrolyte ions.

Sodium *p*-toluenesulfonate (NapTS, 98%) and sodium sulfate anhydrous (Na_2SO_4, 99.5%) were purchased from Merck and BDH Chemicals, respectively.

2.2. Preparation of GO

GO was synthesized using simplified Hummer's method [20]. Graphite oxide was obtained by the oxidation of 3 g of graphite flakes with H_2SO_4:H_3PO_4 (360:40 ml) and 18 g of $KMnO_4$. The mixing process, using a magnetic stirrer, normally required less than 5 min to complete. However, to ensure complete oxidation of graphite, the mixture was stirred for 3 days. During the oxidation process, the color of the mixture changed from dark purplish-green to dark brown. H_2O_2 solution was added to stop the oxidation process, in which the color of the mixture changed to bright yellow, indicating a high oxidation level of the graphite. The graphite oxide formed was washed with 1 M of HCl aqueous solution, and subsequently with de-ionized water (repeatedly), until a pH of 4–5 was achieved. The washing process was conducted *via* simple decantation of the supernatant, using the centrifugation technique. During the washing process with de-ionized water, the graphite oxide experienced exfoliation, which resulted in the thickening of the GO solution, and ultimately formed GO gel. The concentration of the GO gel was 4.38 mg/ml.

2.3. Preparation of PPy/GR/MnO_x nanocomposite film

PPy/GR/MnO_x nanocomposite films were deposited onto indium tin oxide (ITO)-coated glass, by potentiostatic deposition from an aqueous solution placed in a one-compartment cell. The deposition solution contained 0.1 M of pyrrole, 1 mg/ml of GO, 0.1 M of NapTS, and 0.1–0.5 M of $MnSO_4$. A potentiostat-galvanostat (Elchema model EQCN-502 Faraday cage) was used for the synthesis of the nanocomposite films at room temperature. A graphite electrode was used as a counter-electrode, while the working electrode was ITO. A saturated calomel electrode (SCE) was used as the reference electrode. The electrochemical deposition was performed at a constant potential of +0.8 V (versus SCE) for 2 h. For comparison purposes, PPy film and PPy/GR film were also synthesized.

2.4. Materials characterizations

X-ray photoelectron spectroscopy (XPS) measurement was carried out using Axis Ultra^{DLD} (Kratos Analytical Ltd.). The crystalline structure of the samples was analyzed using Siemens D5000 X-ray diffraction (XRD), while Fourier Transform infrared (FT-IR) spectra were recorded on a Perkin-Elmer FT-IR spectroscopy model 1725x. The surface morphology of samples was investigated using a field emission scanning electron microscopy (FESEM, FEI Nova NanoSEM 400).

2.5. Electrochemical measurements

To understand the electrochemical performance of the nanocomposite electrode, the electrochemical properties of the materials were measured using the VersaSTAT 3 electrochemical system (Princeton Applied Research). Cyclic voltammetry (CV), galvanostatic charge/discharge and electrochemical impedance spectroscopy (EIS) were all carried out using a three-electrode cell system, in which nanocomposite films were used as the working electrode, platinum wire as a counter-electrode and Ag/AgCl as the reference electrode. CV was conducted between −0.2 and 0.7 V (versus Ag/AgCl), at scan rates between 1 and 100 mV/s. The specific capacitance values of the samples were calculated from cyclic voltammograms using Eq. (1) [21]

$$Cm = \frac{\int i}{ms} \quad (1)$$

where Cm is the specific capacitance in farads per gram, $\int i$ is the integrated area of the CV curve, m is the mass of the electrode material in grams, and S is the scan rate in volts per second. Galvanostatic charge/discharge was conducted between −0.2 and 0.7 V (versus Ag/AgCl), at a current density of 1 A/g, while the long-term cycling performances of the PPy/GR and PPy/GR/0.1 M MnO_x electrodes were measured by consecutive galvanostatic charge/discharge at a current density of 1 A/g for 1000 cycles. EIS was carried out between 100 KHz and 10 mHz, with an AC amplitude of 5 mV.

3. Results and discussion

This work essentially demonstrated an electrochemical doping-deposition route for simultaneous doping of PPy with pTS ions, and embedding of MnO_x and GR. The XRD patterns of all the samples are shown in Fig. 2. In Fig. 2a, the characteristic peak of PPy can be observed at 16°, which corresponds to pyrrole counter ion or inter-counter ion interaction scattering, while the peak at 22.8° is assigned to the PPy chain that is close to the inter-planar Van de Waals distance from the aromatic groups [22]. The overall features of the XRD pattern of PPy/GR nanocomposite film are very similar to those of PPy, indicating that no additional crystalline phase has been introduced into the nanocomposite [23]. At a low concentration of $MnSO_4$, the XRD pattern of the nanocomposite is similar to that of free PPy. This is attributed to the scarce distribution of oxide particles on the surface of the nanocomposite, as a consequence of which the XRD peaks of PPy are predominant. With the increase of MnO_x concentration in the PPy/GR/MnO_x nanocomposite, there are distinguishable diffraction peaks assigned to MnO_2 (JCPDS no. 44-0141) and Mn_2O_3 (JCPDS no. 41-1442), i.e. 12.8°, 25.8°, 29.9°, 39.1° and 50.0° for MnO_2, while 18.9° and 55.4° are attributed to Mn_2O_3, indicating that the nanocomposite contains mixed manganese oxide (Fig. 2b). The intensity of the manganese oxide peaks is weak, implying a marginal degree of crystallization. Therefore, this can be construed as a typical amorphous structure [24], which has the potential to be used as supercapacitor electrode material [25].

To afford a more complete understanding of the surface characteristics of the samples, the PPy/GR/0.1 M MnO_x nanocomposite was analyzed further using XPS. The presence

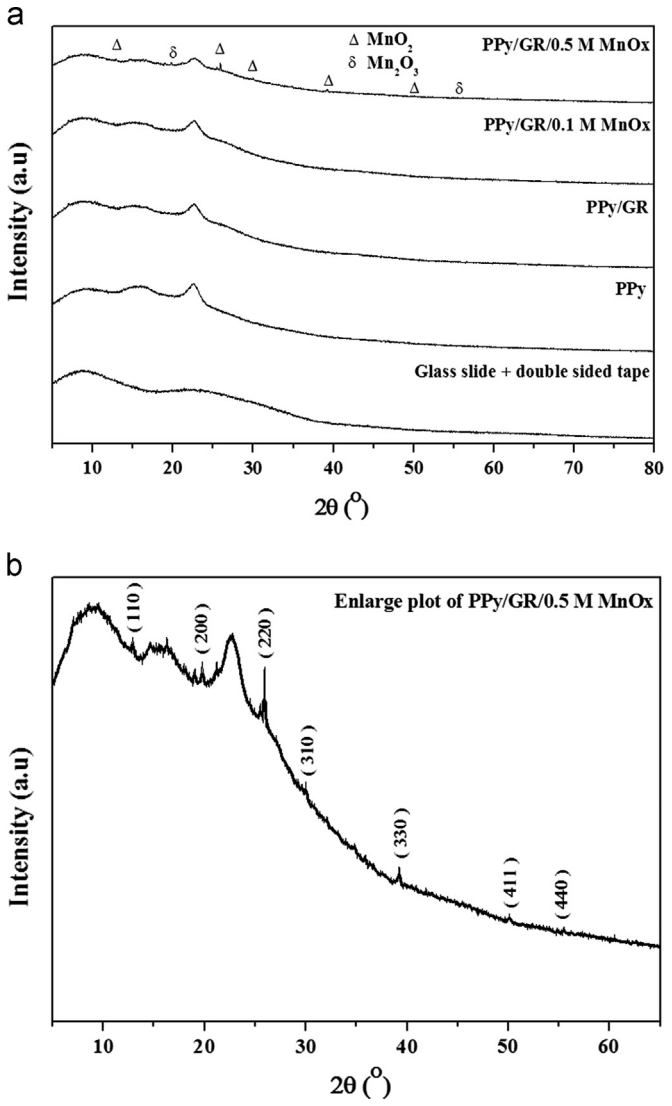

Fig. 2. (a) XRD diffraction peak of: glass slide with double-sided tape, PPy, PPy/GR; PPy/GR0.1 M MnO_x; and PPy/GR/0.5 M MnO_x and (b) enlarged XRD diffraction peak of PPy/GR/0.5 MnO_x.

of Mn oxide within the matrix of PPy/GR/MnO_x is evident from the Mn signals. Since the contribution of the Mn-oxide component as a pseudocapacitor has a direct impact on the overall electrochemical performance of the nanocomposites, precise knowledge of the oxidation state of Mn is thus required. Fig. 3a displays the Mn 2*p* core level spectrum, which shows broad peaks of Mn $2p_{3/2}$ and Mn $2p_{1/2}$, indicating that the nanocomposite consists of mixed Mn species at various oxidation states. Mn $2p_{3/2}$ and Mn $2p_{1/2}$ have been deconvoluted into four components peaks. In this case, 641.3 and 653.2 eV are attributed to Mn^{3+}, while 642.3 and 654.2 eV are attributed to Mn^{4+}, suggesting that there are mixed valence states of Mn^{3+} and Mn^{4+}. Taking into consideration the XRD observation, this implies the formation of Mn_2O_3 and MnO_2, respectively [26]. Therefore, the prepared manganese oxide is a mixed-manganese oxide, and responsible for the amorphous structure of MnO_2 and Mn_2O_3 [12]. The areas under the associated peaks reveal the relative amounts of these components, whereby MnO_2 (57%) is the dominant form. The existence of Mn oxides is also reflected in the O_{1s} core level spectrum, as shown in Fig. 3b. The spectrum can be deconvoluted into four components, which are related to Mn–O–Mn oxide (530.4 eV) [3], C–O or S–O (531.4 eV), COOH (533.7 eV) [27], and H–O–H (532.7 eV) [28]. The C–O and COOH bonds are remnants of the oxide functional groups of the GO, whereas the S–O bond originates from NapTS as a dopant. The XPS C_{1S} core level spectrum of the nanocomposite film can be fitted into six component peaks, with binding energies of 284.2, 284.6, 285.2, 286.2, 287.3 and 288.6 eV, which are attributed to the sp^2 hybridized carbon, sp^3 hybridized carbon [29], C–N[30], C–O, C=O and COOH [31], respectively. The carboxyl and carboxylic groups are the remaining oxygenous groups of the GO.

The FT-IR spectra of GO and PPy/GR/MnO_x are shown in Fig. 4. The GO spectrum in Fig. 3a shows a broad and intense peak at 3355 cm^{-1}, which corresponds to the OH band. The peak at 1723 cm^{-1} and the peaks in the range of 1400–1000 cm^{-1} are assigned to C–O functionalities; namely, COOH and COC/C–OH, respectively. Since the absorption peaks are close to one another, they overlap, resulting in poorly defined peaks. The peak at 1617 cm^{-1} is associated with the sp^2 character of GO [32]. The nanocomposite spectrum illustrates the characteristic of pure PPy at 1400 cm^{-1} (aromatic ring stretching of pyrrole ring), 996 cm^{-1}(N–H out-of-plane bending) [33] and 1104 cm^{-1} (C–N stretching) [32]. The bands at 700 and 632 cm^{-1} can be ascribed to the Mn–O vibration of the Mn (IV)–O in MnO_2 and Mn (III)–O in Mn_2O_3 [25,34–36]. This provides evidence for the oxidation of Mn^{2+} into MnO_2 and Mn_2O_3 in the nanocomposite during the electrodeposition process. These results suggest that MnO_2 and Mn_2O_3 are present within the matrix of PPy/GR/MnO_x. Moreover, the characteristic of oxygen functionalities disappears, indicating that the GO has been reduced to GR. From the XPS and FT-IR analyses, we deduced that the oxidation of Mn^{2+} and pyrrole monomers would significantly reduce GO to GR.

Fig. 5 illustrates the FESEM images of PPy, PPy/GR and PPy/GR/MnO_x. PPy has a typical granule-like surface (Fig. 5a), whereas PPy/GR consists of a network structure of fibre-like morphology (Fig. 5b). The cross-sectional view of PPy/GR film shows that GR and PPy were condensed into a new entity, with no clear distinction of a single component (Fig. 5c). The presence of MnO_x gives rise to a notable porous structure, as it acted as a spacer to prevent the stacking of graphene sheets [37], as shown in Fig. 5d and e. The high magnification image of PPy/GR/0.1 M MnO_x (Fig. 5f) clearly shows the integration of MnO_x nodular nanograins on the graphene sheet, whereby the diameter of nodular grains ranges from 10 nm to 100 nm, hence affording a porous 3D structure. However, in PPy/GR/0.5 M MnO_x (Fig. 5g), MnO_x is formed, with an icicle-like morphology. The presence of Mn for PPy/GR/0.1 M MnO_x is evident in the EDX spectrum (Fig. 5h). The area of bright contrast correlates to the Mn signal map in Fig. 5i. This result, coupled with the XRD and XPS results,

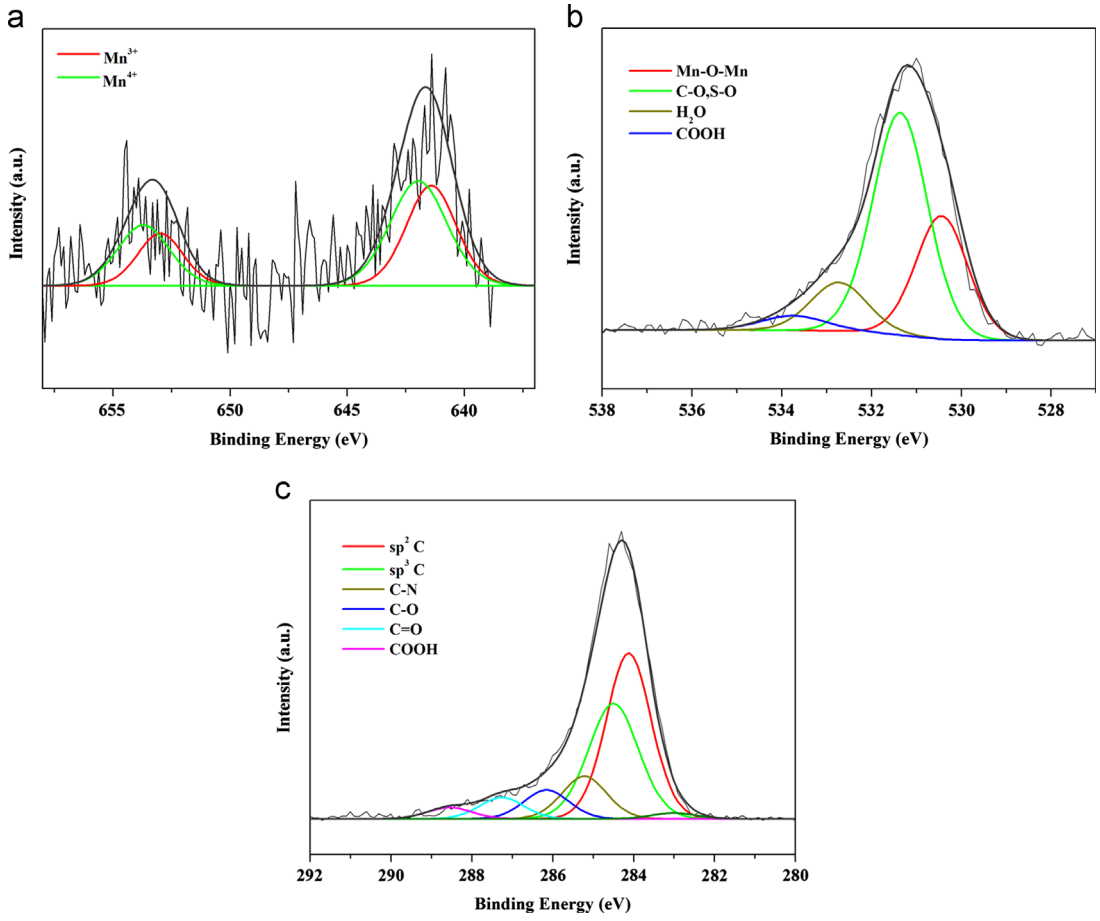

Fig. 3. XPS spectra of PPy/GR/0.1 M MnO_x at: (a) Mn 2*p*; (b) O 1*s*; and (c) C 1*s* region.

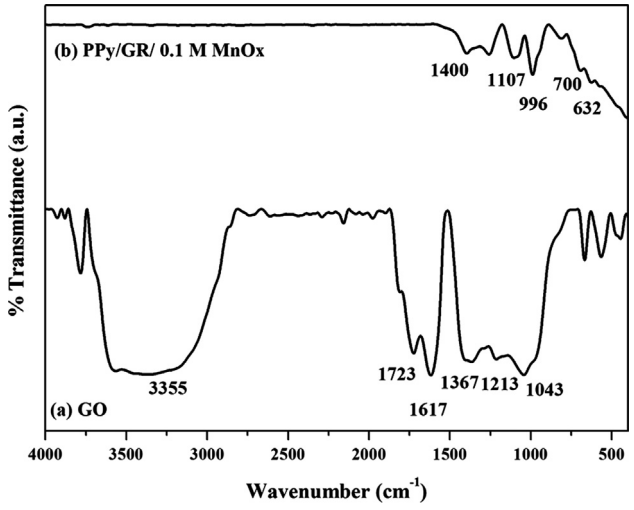

Fig. 4. FT-IR spectra of: (a) GO; and (b) PPy/GR/0.1 M MnO_x.

provides evidence for the presence of MnO_x particles in the ternary nanocomposite.

Based on the above considerations, one would expect 3D PPy/GR/MnO_x to facilitate electrolyte penetration, and the capacitive behavior can be reflected from the CV profile. Generally, CV with a higher current response corresponds to higher specific capacitance. CV curves recorded for PPy, PPy/GR and PPy/GR/0.1 M MnO_x electrodes are shown in Fig. 6. The PPy/GR/MnO_x electrode exhibits a high output current in comparison with those of PPy and PPy/GR, indicating an enhancement of charge storage in the ternary nanocomposite. The voltammogram of PPy/GR/0.1 M MnO_x nanocomposite is fairly rectangular without obvious redox peaks, indicating that the nanocomposite has ideal capacitive behavior. The calculated specific capacitances of PPy/GR/0.1 M MnO_x, PPy/GR and PPy are 320.6 F/g, 255.1 and 118.4 F/g, respectively. The superior charge storage of the binary nanocomposite over PPy is a result of the synergistic effects between graphene and PPy. The incorporation of GR into PPy decreases the distance for electron shuttling during the electrochemical reaction, as graphene enhances the electronic conductive channel, rendering fast transportation of electrons in the PPy/GR modified electrode [38].

The excellent electrochemical performance of PPy/GR/0.1 M MnO_x compared with PPy/GR is attributed to the structural modifications of the ternary nanocomposite. This implies that the MnO_x played an important role during the growth of the film, leading to the formation of unique morphology that enhanced the performance of the ternary

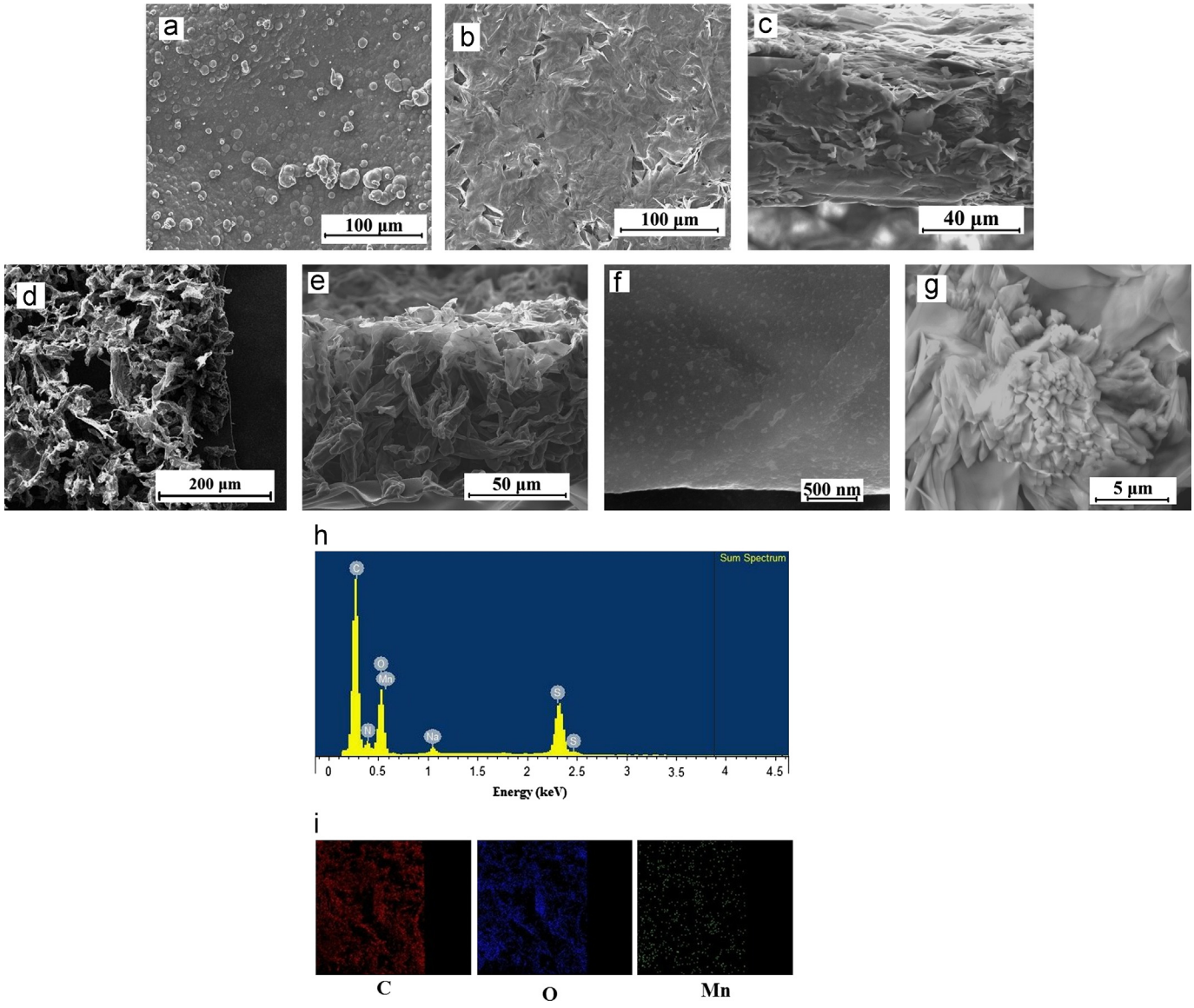

Fig. 5. FESEM images of: (a) PPy; (b) PPy/GR; (c) cross-sectional view of PPy/GR; (d) PPy/GR/0.1 M MnO_x; (e) cross-sectional view of PPy/GR/0.1 M MnO_x; (f) high magnification PPy/GR/0.1 M MnO_x; and (g) high magnification PPy/GR/0.5 M MnO_x; (h) EDX spectrum of PPy/GR/0.1 M MnO_x; and (i) elemental mapping of PPy/GR/0.1 M MnO_x, based on image shown in (d).

nanocomposite. During the growth of the PPy/GR/MnO_x nanocomposite, MnO_x particles coated the surfaces of individual graphene sheets, and acted as a spacer to prevent the restacking of graphene sheets. This caused the sheets to stack and form a porous, three-dimensional structure. Such morphology is most effective in facilitating the diffusion of electrolyte within the matrix. Moreover, the nanoscale size of the MnO_x particles within the nanocomposite increased its electrochemical capability significantly, owing to its high active surface area. Therefore, this nanocomposite is a promising candidate for the construction of a high performance supercapacitor electrode. Two mechanisms have been proposed for charge-storage in Faradaic redox MnO_2-based electrodes [39,40]. The first is built on the aspect of rapid intercalation of alkali metal cations such as Na^+ in the electrode during reduction, and deintercalation upon oxidation, where C^+=Na^+ and H^+ and the proposed mechanism involves a redox reaction between the III and IV oxidation states of Mn

$$MnO_2+C^+ + e^- \leftrightarrow MnOOC \quad (2)$$

The second mechanism concerns the adsorption of cations on the electrode surface from electrolyte

$$(MnO_2)_{surface}+C^+ \leftrightarrow (MnOO^-C^+)_{surface} \quad (3)$$

Fig. 7 shows the effect of $MnSO_4$ concentration on the electrochemical performance of nanocomposite. The specific capacitances of the nanocomposites increased from 273.5 to 320.6 F/g, when respective concentrations of 0.05 M and 0.1 M of $MnSO_4$ were used for the preparation of the nanocomposites. This can be attributed to the nano-sized MnO_x particles. When produced at the optimized concentration

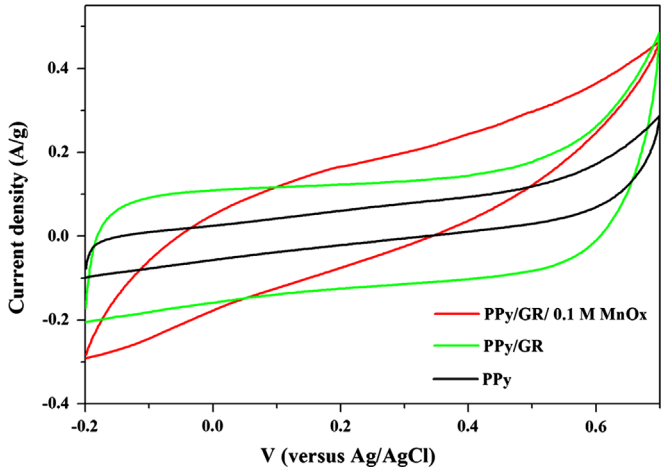

Fig. 6. CVs for PPy, PPy/GR and PPy/GR/0.1 M MnO_x at a scan rate of 1 mV/s.

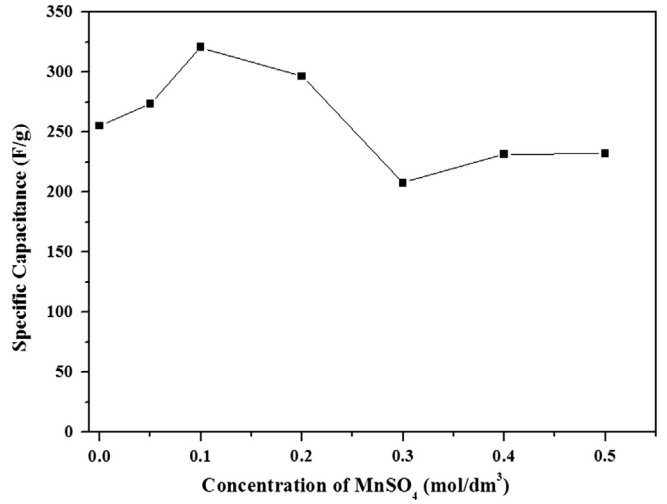

Fig. 7. Specific capacitance for different concentrations of $MnSO_4$ at scan rate of 1 mV/s.

of 0.1 M of $MnSO_4$, they act as spacers for the PPy-coated GR sheets which promote the penetration of electrolyte. This gives rise to a large redox-active surface area and contributes to the material's pseudocapacitance, in addition to the pseudocapacitance from PPy and EDLC from GR. Further increase of the $MnSO_4$ concentration attenuates the charge storage performance of the nanocomposites. The specific capacitances of the nanocomposites decrease progressively from 320.6 to 296.4 F/g, and ultimately, 207.6 F/g, when respective concentrations of 0.1 M, 0.2 M and 0.3 M of $MnSO_4$ were used for the preparation of the nanocomposites. The deteriorating performance of the nanocomposite is due to the presence of bulk MnO_x because a higher concentration of $MnSO_4$ leads to the deposition of bulk MnO_x, as illustrated in Fig. 5g. This reduces the MnO_x-electrolyte interfacial area, a detrimental phenomenon for ion kinetics, which lowers the charge storage properties. With the use of 0.4 and 0.5 M of $MnSO_4$ for the preparation of the nanocomposites, they exhibit a paltry increase to 231.4 and 232.3 F/g due to the increasing loading of bulk MnO_x. This is typically the specific capacitance exhibited by that of bulk MnO_x (~125–250 F/g) [41].

The influence of the scan rate is minimal with respect to the electrochemical performance of the ternary nanocomposite (Fig. 8). Even though the current density increases with scan rate, the rectangular shape of the CV curves remains the same. This corresponds to the rapid current response on voltage reversal at each potential end, following the ideal capacitive behavior. The slight deviation from rectangularity for the CV curve at 100 mV/s is attributed to the reduction of effective interaction between the ions and the electrode at the high scan rate, owing to lesser charge mobilization per unit time.

Near-ideal EDLC behavior of the charge/discharge curves is seen by the symmetric charge and discharge slopes, where a triangle curve is observed [42] (Fig. 9). This behavior is desirable because this implies that the electrode has excellent electrochemical reversibility and charge/discharge properties. The slight curvatures of the slopes of the PPy and PPy/GR electrodes are indicative of the involvement of the Faradaic

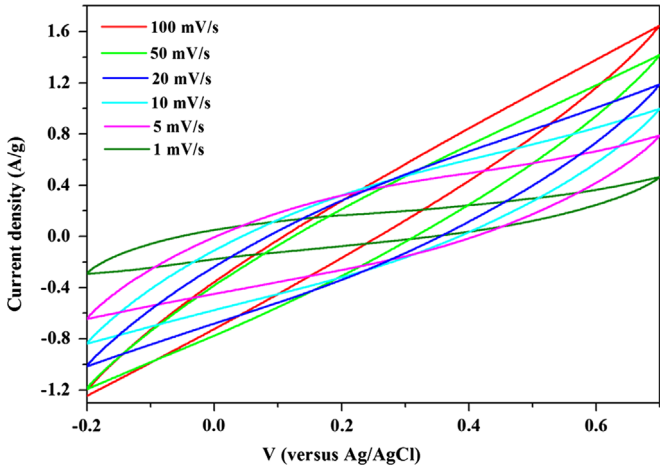

Fig. 8. CVs of PPy/GR/0.1 M MnO_x at different scan rates.

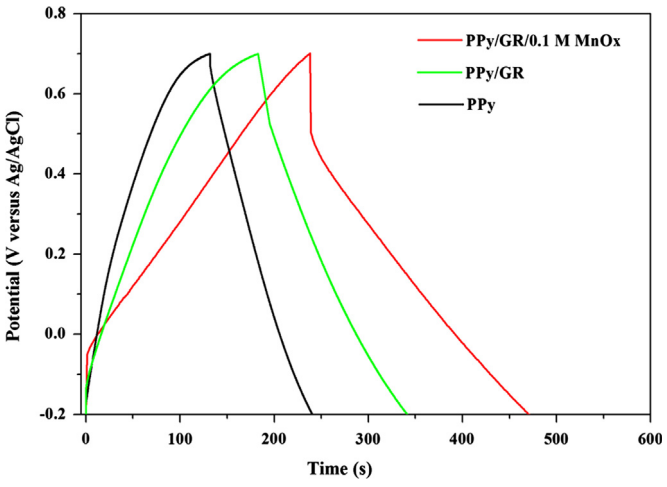

Fig. 9. Galvanostatic charge/discharge curves of PPy/GR/0.1 M MnO_x, PPy/GR and PPy at a current density of 1 A/g.

reaction process of the PPy [43] and, naturally, the curvature becomes more pronounced for PPy/GR/0.1 M MnO_x. This indicates the additional contribution of pseudocapacitance to the system as a result of the presence of MnO_x in the electrode matrix.

Electrochemical impedance spectroscopy (EIS) is performed to investigate the resistive components of the nanocomposite electrodes involved in the electrochemical system. A Nyquist plot (Fig. 10) of PPy/GR and PPy/GR/MnO_x shows a small semi-circle at high-medium frequency, presented in the lower left portion of the spectra, followed by a vertical line along the imaginary axis in the low frequency region. This can be represented by three major processes and the equivalent circuit, in accordance with the Nyquist plot presented (Fig. 10, inset). This equivalent circuit consists of an equivalent series resistance (ESR), in series with the parallel combination of the double layer capacitance C_{dl} and an impedance of the Faradaic reaction. The latter consists of a charge transfer resistance (R_{ct}), owing to a Faradaic redox process in the system involving the exchange of Na^+, and a diffusive resistance (W) corresponding to the diffusion of Na^+ ions. A pure capacitive behavior (C_{dl}) is represented in the low frequency region, in which an almost vertical line is observed. The first intercept point of the semi-circle on the real axis (Z') represents equivalent series resistance (ESR). This value is attributed to the identical combination of electrolyte, internal resistance of the electrode and the contacts between the electrode and current collector [44]. The ESR is determined to be 42.9 Ω PPy/GR/0.1 M MnO_x, which is higher than that of PPy/GR, 31.3 Ω. Moreover, it is found that the ESR is increased to 48.3 Ω for PPy/GR/0.5 M MnO_x, implying that the electrode is more resistive with the increase of Mn-oxide amount in the nanocomposites. This change is caused by the poor electronic conductivity of MnO_2 [41]. The R_{ct} of PPy/GR/0.1 M MnO_x (1.4 Ω) and PPy/GR/0.5 M MnO_x (1.4 Ω) estimated from the diameter of the semi-circle are higher than PPy/GR (0.9 Ω). Such a change in R_{ct} is consistent with the fact that inclusion of insulating Mn oxide in conducting carbon electrode leads to an increased R_{ct} [45,46].

A long cycling life is an important parameter for evaluation of the applicability of a supercapacitor material. Fig. 11 shows the cycling performances of the two nanocomposites at 1 A/g in a galvanostatic charge/discharge test. The specific capacitance of PPy/GR/0.1 M MnO_x decreases by ~7%, while that of PPy/GR electrode decreases by ~11% after 1000 cycles, indicating a good cycling life of the PPy/GR/0.1 M MnO_x. The rapid decrease in the specific capacitance of PPy/GR electrode indicates that it has a lower electrochemical stability in charge/discharge cycling than the PPy/GR/0.1 M MnO_x nanocomposite. This deterioration in the electrode performance is attributed to the mechanical and electrical faults in the polymer chains, owing to the continuous volume expansion/contraction of electrode during the charge/discharge cycles. However, the stability of PPy/GR/0.1 M MnO_x is enhanced because the MnO_x adhered in the nanocomposite matrix inhibits the gradual structural deterioration of nanocomposite, which may result from the repetitive polymer swelling/shrinking during the charge/discharge processes. Thus, the co-deposited MnO_x increases the electrochemical performance and improves stability.

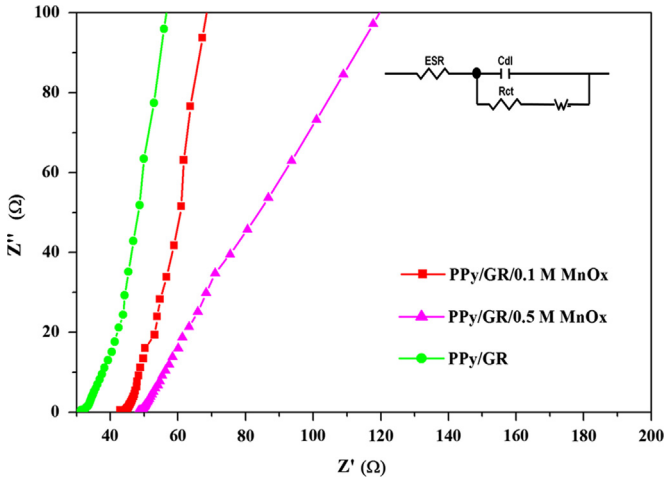

Fig. 10. Nyquist plot of PPy/GR/0.1 M MnO_x, PPy/GR/0.5 M MnO_x and PPy/GR.

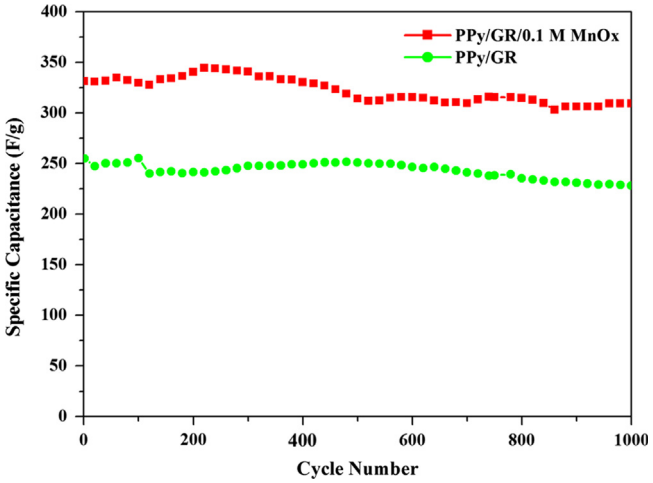

Fig. 11. Specific capacity retention for PPy/GR/0.1 M MnO_x and PPy/GR electrodes at a charge/discharge current density of 1 A/g.

4. Conclusions

A simple approach based on potentiostatic polymerization was developed for the preparation of ternary manganese-oxide-based nanocomposite films. This approach involves the controlled synthesis of salt precursors (manganese sulfate in this case) at various concentrations. This strategy can be extended to other types of precursors for the preparation of different types of nano-sized oxides. The prepared manganese-oxide-based nanocomposite films are non-stoichiometric and responsible for the amorphous structure of MnO_2 and Mn_2O_3. The PPy/GR/MnO_x ternary nanocomposite film, prepared at a lower MnO_x concentration, has a higher specific capacitance, owing to the contribution of the redox process of co-deposited MnO_x particles. The PPy/GR/MnO_x ternary nanocomposite has promising electrochemical stability, with a long and stable life span for 1000 cycles.

Acknowledgments

The author would like to acknowledge Universiti Putra Malaysia for the Graduate Research Fellowship. This research was supported by a UMRG research grant from the University of Malaya (RG11711AFR), and a High Impact Research Grant from the Ministry of Higher Education (UM.C/625/1/HIR/MOHE/05).

References

[1] P. Jampani, A. Manivannan, P.N. Kumta, Advancing the supercapacitor materials and technology frontier for improving power quality, Electrochemical Society Interface 19 (2010) 57–63.
[2] M. Jin, G. Han, Y. Chang, H. Zhao, H. Zhang, Flexible electrodes based on polypyrrole/manganese dioxide/polypropylene fibrous membrane composite for supercapacitor, Electrochimica Acta 56 (2011) 9838–9845.
[3] R.K. Sharma, A.C. Rastogi, S.B. Desu, Manganese oxide embedded polypyrrole nanocomposites for electrochemical supercapacitor, Electrochimica Acta 53 (2008) 7690–7695.
[4] Q. Li, Z. Li, L. Lin, X.Y. Wang, Y. Wang, C. Zhang, H. Wang, Facile synthesis of activated carbon/carbon nanotubes compound for supercapacitor application, Chemical Engineering Journal 156 (2010) 500–504.
[5] D.A.C. Brownson, D.K. Kampouris, C.E. Banks, An overview of graphene in energy production and storage applications, Journal of Power Sources 196 (2011) 4873–4885.
[6] D.A.C. Brownson, C.E. Banks, Graphene electrochemistry: an overview of potential applications, Analyst 135 (2010) 2768–2778.
[7] D.R. Dreyer, S. Park, C.W. Bielawski, R.S. Ruoff, The chemistry of graphene oxide, Chemical Society Reviews 39 (2010) 228–240.
[8] M. Pumera, Electrochemistry of graphene: new horizons for sensing and energy storage, Chemistry Record 9 (2009) 211–223.
[9] C.O. Yoon, H.K. Sung, J.H. Kim, E. Barsoukov, J.H. Kim, H. Lee, The effect of low-temperature conditions on the electrochemical polymerization of polypyrrole films with high density, high electrical conductivity and high stability, Synthetic Metals 99 (1999) 201–212.
[10] K.S. Ryu, Y. Lee, Y. Hong, Y.J. Park, X. Wu, K.M. Kim, M.G. Kang, N. Park, S.H. Chang, Poly(ethylenedioxythiophene) (PEDOT) as polymer electrode in redox supercapacitor, Electrochimica Acta 50 (2004) 843–847.
[11] H. An, Y. Wang, X. Wang, L. Zheng, X. Wang, L. Yi, L. Bai, X. Zhang, Polypyrrole/carbon aerogel composite materials for supercapacitor, Journal of Power Sources 195 (2010) 6964–6969.
[12] F. Liu, T. Hsu, C. Yang, Construction of composite electrodes comprising manganese dioxide nanoparticles distributed in polyaniline-poly(4-styrene sulfonic acid-co-maleic acid) for electrochemical supercapacitor, Journal of Power Sources 191 (2009) 678–683.
[13] S. Chen, J. Zhu, X. Wu, Q. Han, X. Wang, Graphene oxide-MnO_2 nanocomposites for supercapacitors, ACS Nano 4 (2010) 2822–2830.
[14] H. Yang, J. Jiang, W. Zhou, L. Lai, L. Xi, Y. Lam, Z. Shen, B. Khezri, T. Yu, Influences of graphene oxide support on the electrochemical performances of graphene oxide-MnO_2 nanocomposites, Nanoscale Research Letters 6 (2011) 1–8.
[15] G. Wang, L. Zhang, J. Kim, J. Zhang, Nickel and cobalt oxide composite as a possible electrode material for electrochemical supercapacitors, Journal of Power Sources.
[16] G.A. Snook, P. Kao, A.S. Best, Conducting-polymer-based supercapacitor devices and electrodes, Journal of Power Sources 196 (2011) 1–12.
[17] J.W. Lee, A.S. Hall, J. Kim, T.E. Mallouk, A facile and template-free hydrothermal synthesis of Mn_3O_4 nanorods on graphene sheets for supercapacitor electrodes with long cycle stability,, Chemistry of Materials 24 (2012) 1158–1164.
[18] J. Zhang, J. Jiang, X.S. Zhao, Synthesis and capacitive properties of manganese oxide nanosheets dispersed on functionalized graphene sheets, Journal of Physical Chemistry C 115 (2011) 6448–6454.
[19] Y.S. Lim, Y.P. Tan, H.N. Lim, W.T. Tan, M.A. Mahnaz, Z.A. Talib, N.M. Huang, A. Kassim, M.A. Yarmo, Polypyrrole/graphene composite films synthesized via potentiostatic deposition, Journal of Applied Polymer Science 128 (2013) 224–229.
[20] N.M. Huang, H.N. Lim, C.H. Chia, M.A. Yarmo, M.R. Muhammad, Simple room-temperature preparation of high-yield large-area graphene oxide, International Journal of Nanomedicine 6 (2011) 3443–3448.
[21] J. Wang, Y. Xu, X. Chen, X. Du, Electrochemical supercapacitor electrode material based on poly(3,4-ethylenedioxythiophene)/polypyrrole composite, Journal of Power Sources 163 (2007) 1120–1125.
[22] K. Cheah, M. Forsyth, V. Truong, Ordering and stability in conducting polypyrrole, Synthetic Metals 94 (1998) 215–219.
[23] A. Liu, C. Li, H. Bai, G. Shi, Electrochemical deposition of polypyrrole/sulfonated graphene composite films, Journal of Power Sources 114 (2010) 22783–22789.
[24] A.H. Gemeay, R. El-Sharkawy, I.A. Mansour, A.B. Zaki, Preparation and characterization of polyaniline/manganese dioxide composites and their catalytic activity, Journal of Colloid and Interface Science 308 (2007) 385–394.
[25] H. Zhang, Y. Wang, C. Liu, H. Jiang, Influence of surfactant CTAB on the electrochemical performance of manganese dioxide used as supercapacitor electrode material, Journal of Alloys and Compounds 517 (2012) 1–8.
[26] G.C. Allen, S.J. Harris, J.A. Jutson, J.M. Dyke, A study of a number of mixed transition metal oxide spinels using X-ray photoelectron spectroscopy, Applied Surface Science 37 (1989) 111–134.
[27] S.C. Ray, A. Saha, S.K. Basiruddin, S.S. Roy, N.R. Jana, Polyacrylate-coated graphene-oxide and graphene solution via chemical route for various biological application, Diamond and Related Materials 20 (2011) 449–453.
[28] L. Sun, X. Liu, K.K. Lau, L. Chen, W. Gu, Electrodeposited hybrid films of polyaniline and manganese oxide in nanofibrous structures for electrochemical supercapacitor, Electrochimica Acta 53 (2008) 3036–3042.
[29] J. Zhang, Y. Yu, D. Huang, Good electrical and mechanical properties induced by the multilayer graphene oxide sheets incorporated to amorphous carbon films, Solid State Science 12 (2010) 1183–1187.
[30] S. Bose, T. Kuila, M.E. Uddin, N.H. Kim, A.K.T. Lau, J.H. Lee, In-situ synthesis and characterization of electrically conductive polypyrrole/graphene nanocomposites, Polymer 51 (2010) 5921–5928.
[31] S. Yumitori, Correlation of C1s chemical state intensities with the O1s intensity in the XPS analysis of anodically oxidized glass-like carbon samples, Journal of Materials Science 35 (2000) 139–146.
[32] Y. Han, L. Hao, X. Zhang, Preparation and electrochemical performances of graphite oxide/polypyrrole composites, Synthetic Metals 160 (2010) 2336–2340.
[33] S. Jamadade, S.V. Jadhav, V. Puri, Electromagnetic reflection, shielding and conductivity of polypyrrole thin film electropolymerized in P-Tulensulfonic acid, Journal of Non-Crystalline Solids 357 (2011) 1177–1181.
[34] X. Yang, Y. Makita, Z. Liu, K. Sakane, K. Ooi, Structural characterization of self-assembled MnO_2 nanosheets from birnessite manganese oxide single crystals, Chemistry of Materials 16 (2004) 5581–5588.
[35] R. Yang, Z. Wang, L. Dai, L. Chen, Synthesis and characterization of single-crystalline nanorods of α-MnO_2 and γ-MnOOH, Materials Chemistry and Physics 93 (2005) 149–153.
[36] T.K. Ghorai, S. Pramanik, P. Pramanik, Synthesis and photocatalytic oxidation of different organic dyes by using Mn_2O_3/TiO_2 solid solution and visible light, Applied Surface Science 255 (2009) 9026–9031.
[37] P.S. Teo, H.N. Lim, N.M. Huang, C.H. Chia, I. Harrison, Room temperature in situ chemical synthesis of Fe_3O_4/graphene, Ceramics International 38 (2012) 6411–6416.
[38] Y. Han, B. Ding, X. Zhang, Effect of feeding ratios on the structure and electrochemical performance of graphite oxide/polypyrrole nanocomposites, Chinese Science Bulletin 56 (2011) 2846–2852.
[39] V. Subramanian, H. Zhu, B. Wei, Nanostructured MnO_2: hydrothermal synthesis and electrochemical properties as a supercapacitor electrode material, Journal of Power Sources 159 (2006) 361–364.

[40] M. Toupin, T. Brousse, D. Belanger, Charge storage mechanism of MnO_2 electrode used in aqueous electrochemical capacitor, Chemistry of Materials 16 (2004) 3184–3190.
[41] D. Belanger, T. Brousse, J.W. Long, Manganese oxides: battery materials make the leap to electrochemical capacitors, Electrochemical Society Interface 17 (2008) 49–52.
[42] A.L. Reddy, S. Ramaprabhu, Nanocrystalline metal oxides dispersed multiwalled carbon nanotubes as supercapacitor electrodes, Journal of Physical Chemistry C 111 (2007) 7727–7734.
[43] A. Davies, P. Audette, B. Farrow, F. Hassan, Z. Chen, J. Choi, A. Yu, Graphene-based flexible supercapacitors: pulse-electropolymerization of polypyrrole on free-standing graphene films, Journal of Physical Chemistry C 115 (2011) 17612–17620.
[44] S.K. Meher, P Justin, G.R. Rao, Pine-cone morphology and pseudocapacitive behavior of nanoporous nickel oxide, Electrochimica Acta 55 (2010) 8388–8396.
[45] J. Liu, J. Essner, J. Li, Hybrid supercapacitor based on coaxially coated manganese oxide on vertically aligned carbon nanofiber arrays, Chemistry of Materials 22 (2010) 5022–5030.
[46] Z. Lei, Z. Chen, X.S. Zhao, Growth of polyaniline on hollow carbon spheres for enhancing electrocapacitance, Journal of Physical Chemistry C 114 (2010) 19867–19874.